Egyptian Journal of Chemistry

http://ejchem.journals.ekb.eg/

Cetyltrimethylammonium Bromide@$CoFe_2O_4$ Nanocomposite for Photocatalytic Reduction of Cr(VI) Employing a Simple Colorimetry Assay

Ibtisam Alali[1], Souad A. Elfeky[2]*, Amr A. El-Ella[2], Gamal El-Ghannam[2]*

[1]Chemistry Department, College of Science, Jouf University, P.O.BOX: 2014, Sakaka, Saudi Arabia.
[2]National Institute of Laser Enhanced Sciences (NILES), Department of Laser Applications in Metrology, Photochemistry, and Agriculture (LAMPA), Cairo University, Giza, 12613, Egypt

Abstract

The present study involved the synthesis of a nanocomposite material composed of cobalt ferrite ($CoFe_2O_4$) modified with cetyltrimethyl ammonium bromide (CTAB). The preparation method employed a chemical reduction approach. The structural characterization of the CTAB@$CoFe_2O_4$ nanocomposite was carried out using techniques such as transmission electron microscopy (TEM), Fourier-transform infrared spectroscopy (FTIR), and X-ray diffraction (XRD). The XRD analysis confirmed the single-phase cubic crystal structure of the CTAB@$CoFe_2O_4$ nanocomposite. Additionally, the FTIR spectra provided evidence of the presence of CTAB functional groups within the $CoFe_2O_4$ matrix. The zeta potential measurements revealed a positive surface charge of +17.3 mV for the CTAB@$CoFe_2O_4$ nanocomposite. The application of this nanocomposite material was studied for the reduction of chromium (VI) ions (Cr(VI)) from aqueous solutions using a colorimetric method based on 1,5-diphenylcarbazide dye (DPC). The effects of various parameters, including pH, nanocomposite dosage, and contact time, were investigated to assess their influence on the photoreduction efficiency of the $CoFe_2O_4$/CTAB nanocomposite. Remarkably, at a nanocomposite dosage of 3 mg/mL, 99% reduction of Cr(VI) was achieved at pH3 with a contact time of 150 minutes. These findings indicate the potential of the synthesized $CoFe_2O_4$/CTAB nanocomposite as an efficient material for the elimination of Cr(VI) ions from contaminated water sources. One notable distinction of this method is that it goes beyond solely removing Cr(VI) from water, it also converts it into a non-toxic form.

Keywords: Photocatalytic reduction; CTAB@$CoFe_2O_4$; Cr(VI); Diphenyl carbazide; Contaminated water

1. Introduction

Clean drinking water is a significant challenge, particularly in developing countries where industrial growth has resulted in the generation of increasing amounts of wastewater without adequate management and purification systems [1]. These wastewater streams often contain a variety of contaminants that pose environmental hazards and potential harm to both human and animal health [2]. Among the numerous wastewater contaminants, Cr(VI), is of particular concern due to its mutagenic and carcinogenic properties [3]. Cr(VI) is known to be extremely toxic, even in small doses, highly oxidizing in nature, and long-term exposure causes reproductive toxicity [4]. Cr(VI) can enter the environment through various industrial processes, including painting, furnace lining, tanning, dyeing, photography, and steel manufacturing [3]. When consumed in high doses, Cr(VI) can cause severe acute reactions such as gastrointestinal disorders, hemorrhagic diathesis, and convulsions, which may ultimately lead to cardiovascular shock and even death [5]. To address this environmental concern, scientists have proposed numerous wastewater treatment methods with different chemical and physicochemical properties. Some of the traditional methods include ion-exchange, chemical precipitation, coagulation, membrane processes, reduction, and adsorption [6]. These traditional wastewater treatment methods have certain limitations and may not provide complete removal of Cr(VI), necessitating the development of new and improved approaches. One such promising method is heterogeneous photocatalytic reduction processes, which offer advantages such as cost-effectiveness, high catalytic performance, and the absence of secondary byproduct pollutants [7]. In recent studies, $CoFe_2O_4$ nanoparticles (NPs) have emerged as a notable heterogeneous catalyst for wastewater treatment [8], [9] owing to their unique magnetic properties and chemical stability. The utilization of $CoFe_2O_4$ NPs in heterogeneous photocatalytic reduction processes holds promise for more efficient and effective removal of Cr(VI) from wastewater, thus addressing the environmental and health concerns associated with this compound. Additionally, the $CoFe_2O_4$ NPs catalyst can be simply extracted from the treated wastewater sample by centrifugation for recycling purposes. However, $CoFe_2O_4$ NPs are n-type semiconductor, with small optical band gaps (2.0 eV) making them active under

*Corresponding author e-mail: dr_souad_elfeky@niles.cu.edu.eg (Souad A. Elfeky)
Receive Date: 29 March 2024, Revise Date: 18 May 2024, Accept Date: 05 June 2024
DOI: 10.21608/ejchem.2024.279458.9530

visible light treatment [10]. For applying $CoFe_2O_4$ NPs for the photoreduction of Cr(VI) anions,their surface should be positive. To enhance the photocatalytic efficiency, the surface of $CoFe_2O_4$ NPs was modified using a cationic surfactant called CTAB [11]. CTAB modification is ideal for achieving a positive surface charge on $CoFe_2O_4$ NPs, which is necessary for the efficient reduction of Cr(VI) anions. To monitor the concentration of Cr(VI) during the photocatalytic reduction process, a simple and sensitive colorimetric method based on DPC (diphenyl carbazide) was employed[12]. This method allows for the accurate and specific detection of Cr(VI) in a mineral acid solution. Experiments were performed under different conditions to evaluate the photocatalytic reduction efficiency of Cr(VI) using the CTAB modified $CoFe_2O_4$ NPs as the catalyst. The advantages of using CTABe@$CoFe_2O_4$ NC for the photocatalytic reduction of Cr(VI) are evident in its high efficiency, stability, reusability, versatility, and eco-friendly nature by harnessing the synergistic effects of organic-inorganic hybrid materials[10]. Thus, this approach represents a promising strategy for addressing water pollution challenges associated with toxic heavy metals like Cr(VI), paving the way towards a cleaner and healthier environment.

2. Experimental

All chemicals and reagents were obtained from Sigma-Aldrich (USA) and used without further purification. Cobalt nitrate hexahydrate ($Co(NO_3)_2.6H_2O$) and iron(III) nitrate monohydrate ($Fe(NO_3)_3.9H_2O$) were used as metal ion sources. CTAB (Cetyltrimethylammonium bromide, $C_{19}H_{42}BrN$) was used as a cationic surfactant. Sodium hydroxide (NaOH) was used as a basic co-precipitating agent. Double-distilled deionized water was used throughout the preparations and experiments. Potassium dichromate ($K_2Cr_2O_7$), nitric acid, sulfuric acid, and 1,5diphenylcarbazide were purchased from Fluka Co., Switzerland Pure Chemical Corp., and were of analytical reagent grade. A standard stock solution of Cr(VI) 1g/L was prepared for different dilutions of the photoreduction experiments.

2.1. Synthesis of CTAB/$CoFe_2O_4$Nanoparticles

In this study, $CoFe_2O_4$ nanoparticles (NPs) were synthesized according to the method described in [13][14]applying a series of steps. Firstly, a 0.1 M solution of $Co(NO_3)_2.6H_2O$ was prepared in 50 ml of water. The solution was then stirred for 30 minutes at room temperature (RT). Simultaneously, a 0.2 M solution of $Fe(NO_3)_3.9H_2O$ was prepared in another 50 ml of water, which was also stirred for 30 minutes at RT. The solutions of $Co(NO_3)_2.6H_2O$ and $Fe(NO_3)_3.9H_2O$ were then mixed together and further stirred for an additional 30 minutes at RT. Next, a 50 ml solution of 0.3 M CTAB (cetyltrimethylammonium bromide) in deionized (DI) water was added to the previous mixture then heated to 80°C and stirred vigorously for 1 hour. Following this, NaOH was abruptly added to the solution[15], raising the temperature to 90°C and stirring for another 3 hours. This resulted in the formation of a black precipitate. The precipitate was then washed several times with DI water until a neutral pH was achieved. Finally, the precipitate was dried at 120°C for 12 hours. To remove any remaining moisture content, the dried precipitate was annealed at 200°C for 6 hours. Overall, this synthesis method involved the mixing and stirring of $Co(NO_3)_2.6H_2O$ and $Fe(NO_3)_3.9H_2O$ solutions, addition of CTAB, precipitation with NaOH, washing, and drying, followed by annealing to obtain CTAB/$CoFe_2O_4$ NC.The general mechanism of $CoFe_2O_4$ formation, including thermal decomposition of the precursors, $Co(NO_3)_2.6H_2O$ and $Fe(NO_3)_3.9H_2O$, is shownin the following equation [16].

$$2Fe(NO_3)_3.9H_2O+Co(NO_3)_2.6H_2O+16NaOH \longrightarrow CoFe_2O_4+8NaOH+26H_2O+NaNO_3$$

The CTAB@$CoFe_2O_4$ formation involved the adsorption of CTAB onto the nanoparticle surfaces, forming a protective layer around the nanoparticles, stabilizing them and preventing agglomeration. The CTAB-capping to $CoFe_2O_4$ nanoparticles is formed through a combination of electrostatic interactions, hydrogen bonding, and hydrophobic interactions between the CTAB molecules and nanoparticle surfaces[17].

2.2. Photoreduction Experiment

A photoreduction experiment was conducted by illuminating 100 mL of the Cr(IV) aqueous solution (10^{-3} M/L) with a halogen lamp (50 W/m^2), for a duration of 150 minutes. Three different catalyst amounts (1, 3, and 5 mg/mL) were used to investigate the catalytic photoreduction efficiency. Control experiments were done without light irradiation in the presence of the photocatalyst CTAB/$CoFe_2O_4$ NC or in the presence of light irradiation without the photocatalyst. All experiments were carried out under magnetic stirring (300 RPM).

2.3. Cr(VI) Monitoring

The concentration of Cr(VI) at 10^{-3} M/L was monitored using a colorimetric method with DPC reagent as described by [18]with some modifications. During the photoreduction experiment, 100 µL of Cr(VI) was transferred to a glass vial containing 1 mL of 0.2 M sulfuric acid and1mL of DPC (0.5% w/v). The mixture was shaken and left for 5 minutes before measuring the absorbance at 543 nm against a reagent blank every 15 min.

2.4. Nanocomposites Dose Effect

The photoreduction of Cr(VI) ions was carried out using CTAB/$CoFe_2O_4$ NC catalyst at three different concentrations (1, 2, and 3 mg/mL) to determine the optimal dosage. The experiments were conducted under both dark and artificial light conditions.

2.5. Effect of pH

The effect of pH on the photocatalytic reduction activity of the CTAB/$CoFe_2O_4$ was investigated at three different pH values (3, 5, and 7). HCl and NaOH (0.1 N) were used to adjust the pH of the Cr(VI) samples. During the photoreduction

experiment, 100 mL of 10^{-3} M/L Cr(VI) were mixed with three different amount of catalyst powder (1, 3, and 5 mg/mL). The photoreaction was carried out over the course of 150 minutes with stirring.

2.6. Recycling of Cobalt Ferrite

After the photocatalytic reduction of Cr(VI) was achieved, the photocatalyst CTAB/$CoFe_2O_4$ NPs, were recovered from samples by centrifugation, washed with DI water, dried then reused for further photoreduction experiments to investigate the economic impact of the photocatalytic approach [19].

2.7. Instrumentation

The Zeta potential measurement was done by Malvern Nano ZS. UV-visible absorption spectra were recorded using a double-beam spectrophotometer (JENWAY 6800, Germany). The absorbance was measured within the scan range (200-900 nm). The pH-meter used for this study (HANNA instruments, Germany) was calibrated at pH 4 and 7 with appropriate buffer solutions from Merck, USA. FT-IR spectroscopy analysis was performed using a Bruker spectrometer (Vertex 80, 4000-400 cm^{-1}, USA). X-ray diffraction measurements were carried out using an X'Pert-Pro powder diffractometer from PANalytical, Netherlands. Finally, the shape and size of the prepared nanocomposite were determined using transmission electron microscopy (TEM) with a JEOL JEM-1400 (acceleration voltage of 40 to 120kV from Germany. SEM and EDX analysis were performed using Quattro S (Thermo Scientific USA), Field Emission Environmental Scanning Electron Microscope(FE ESEM).

3. Results and Discussion

3.1. Characterization of CTAB/$CoFe_2O_4$ NC

The FTIR spectra of CTAB and CTAB/$CoFe_2O_4$ NC are presented in Fig. (1). CTAB exhibits two intense peaks at 2800–3000 cm^{-1}, which correspond to the symmetric (2848 cm^{-1}) and asymmetric (2918 cm^{-1}) stretching vibrations of methyl and methylene groups [11]. The weak band at 3445 cm^{-1} arises from the stretching vibration of hydroxyl groups. The bands in the region of 1480 cm^{-1} and 1672 cm^{-1} are attributed to the stretching vibration of N^{+}-CH_3. The bands at 720 and 960 cm^{-1} could be related to -CH_2- rockingand C–N^{+} stretchingvibration respectively[20]. In addition, C-N bands appear in the range 1000-1350 cm^{-1} [21]. In the FTIR spectrum of CTAB/$CoFe_2O_4$ NC, the observed peaks in the range of 655-580 cm^{-1} correspond to the tetrahedral metal ion-oxygen complexes stretching), while the octahedral metal ion-oxygen complexes appear at 420-460 cm^{-1} (Raut et al., 2014). The broadband at 3440 cm^{-1} is likely due to the electrostatic interaction between $CoFe_2O_4$ surface hydroxyl groups and the ammonium moiety in CTAB. The presence of CTAB peaks at 2800–3000 cm^{-1} region along with the shift and broadening of CTAB bands at 1480 cm^{-1}, 1672 cm^{-1} and 960 cm^{-1} (due to hydrogen bonding between CTAB and $CoFe_2O_4$) in CTAB/$CoFe_2O_4$ NC FTIR spectrum confirms the formation of CTAB/$CoFe_2O_4$ NC.

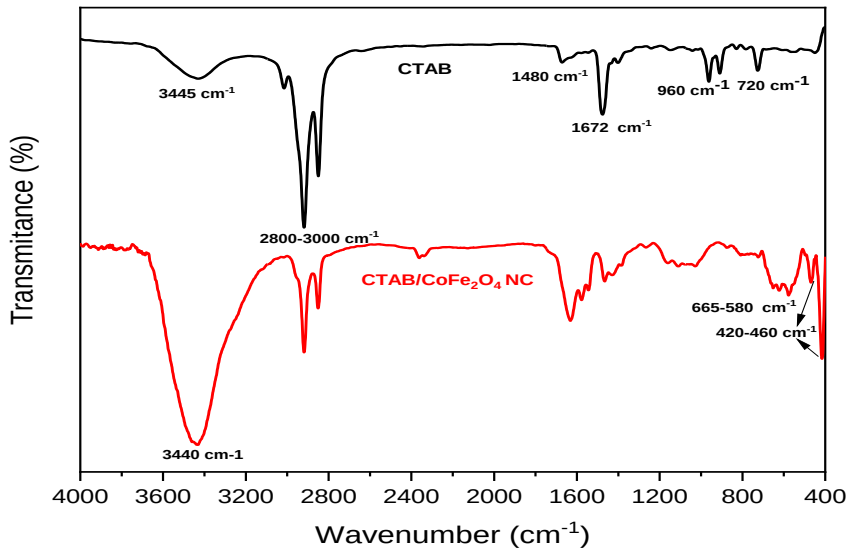

Fig. (1): FTIR spectra of CTAB (black) and the synthesized CTAB/$CoFe_2O_4$ NC (red)

The zeta potential shown in **Fig. (2)** revealed that CTAB/$CoFe_2O_4$ NC has a positive surface charge of +17.3 mV indicating its good stability [22]. In contrast naked $CoFe_2O_4$ NPs have a negative zeta potential value (-13.46 mV) [23]. Thus, capping $CoFe_2O_4$ NPs with cationic surfactant CTAB converted the surface charge to positive.The positive surface charge on $CoFe_2O_4$ nanoparticles is crucial for the efficient reduction of Cr(VI) anions due to several reasons, including, electrostatic attraction, enhanced reactivity, and efficient electron transfer during the reduction of Cr(VI) to Cr(III), leading to improved efficiency of the photo-reduction process and making it an ideal choice for wastewater treatment applications.Based on the XRD diffraction

pattern (**Fig. 3),** it was confirmed that the annealed CTAB/$CoFe_2O_4$ NC has a single-phase cubic crystal structure belonging to the Fd-3m space group. The observed planes (220), (311), (400), (422), (511), and (440) at 2 θ values of 30.2, 35.5, 43.1, 53.5, 57.1, and 62.8º respectively, matched well with the standard JCPDS data reference (card no: 22-1086) [17]. The average crystallite size of cobalt ferrite was calculated to be 19.3 nm applying Scherrer's approximation [24].

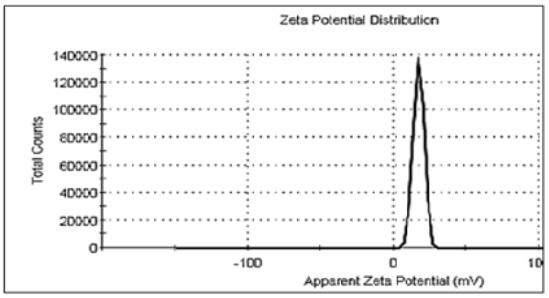

Fig. 2.: Zeta potential of CTAB/CoFe2O4 NC.

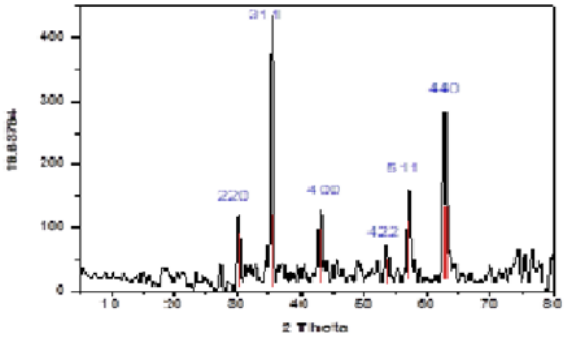

Fig. 3 : X-ray diffraction pattern of annealed CTAB/$CoFe_2O_4$ NC

The SEM images (**Fig. 4 a &b**) and TEM images in **Fig. (4c)** reveal that the as-preparedCTAB/$CoFe_2O_4$ NC consists of aggregated sphere-like nanoparticles due to the surfactant effect [25]**.** The diameters of the nanoparticles range between 15 and 20±5 nm. Additionally, the nanoparticles exhibit a good cubic crystalline structure as displayed in **Fig. (4-c)** which is consistent with the XRD results mentioned earlier.

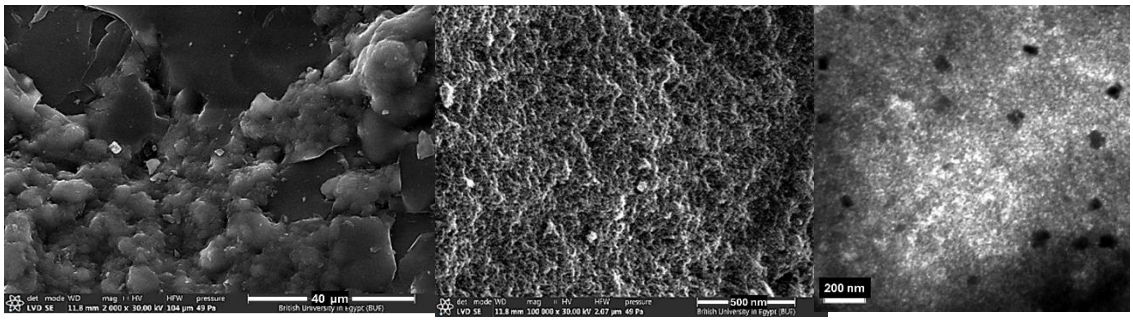

(a) (b) (c)

Fig. (4): Electron microscopy images ofCTAB@$CoFe_2O_4$ NC, (a) and (b) SEM images at two different magnifications 40 µm and 500 nm respectively, and (c) TEM image showing dispersed and cubic crystals of CTAB@$CoFe_2O_4$ NC (scale bar 200 nm).

The existence of Co, Fe, and CTAB elements in CTAB@$CoFe_2O_4$ NC was confirmed by EDX elemental analysis (**Fig. 5**). Fig. (**5-a**) demonstrates that the sample components (Co, Fe, O, C, and N) in area (1) of Fig (**5-b**) are completely matches the anticipated CTAB@$CoFe_2O_4$ NC structure [26][27]. The spectrum also illustrates that the sum of Co/Fe ratio is around 0.5, which is consistent with the formula $CoFe_2O_4$[26].

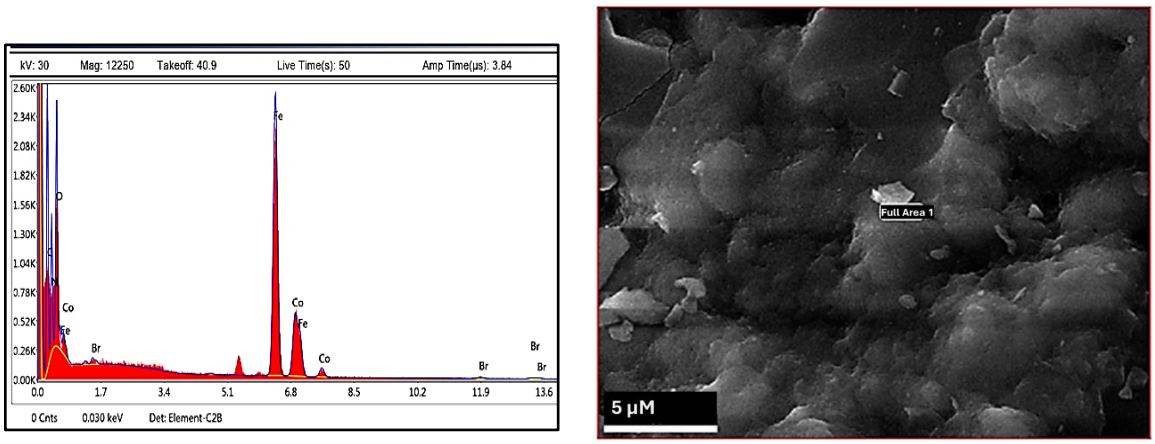

(a) (b)

Fig. (5): EDX analysis of the prepared CTAB@$CoFe_2O_4$ NC (a) showing the elemental mapping of the specific area 1 denoted in the image (b).

The optical absorption spectrum of CTAB@$CoFe_2O_4$ NC demonstrates a broad splittedabsorption peak in the λ = 600–700 nm range **(Fig. 6-a)**. The splitted band between 600-700 nm is characteristic to the tetrahedral Co(II) stereochemistry, indicating the presence of numerous defects in the material, which may contribute to its photocatalytic enhancement [28]. In this arrangement, each metal ion is surrounded by four ligands in a tetrahedral configuration, forming a close-packed structure with a total of eight metal ions in the unit cell. The cobalt ion (Co^{2+}) and two iron ions (Fe^{3+}) are located at the center of a tetrahedron, the four oxygen ions (O^{2-}) act as ligands surrounding each metal ion, forming the vertices of the tetrahedron. The bond angles between the metal ion and the ligands are approximately 109.5 degrees, characteristic of a tetrahedral arrangement [29].

Using the Tauc plot, generated from the UV-vis DRS spectrum, the band gap energy of the CTAB@$CoFe_2O_4$ NC was evaluated **(Fig. 6-b, c)**. The band gap energy can be found at the x-intercept of the extrapolated linear fits (Tatarchuk et al., 2017). The illustrated bandgap has two values: 2.7 eV **(Fig. 6-b)** and 1.7 eV **(Fig. 6-c)**, which most likely correlate to the direct and indirect band gaps, respectively (Duru, 2022). It was reported that a semiconductor having a band gap of 2.7 eV has the ability to absorb solar spectrum blue-violet light with a wavelength of less than 475 nm, making it a promising option for photocatalysis [30]. However, indirect band gap semiconductors are preferable for longer charge carrier lifetimes [31]. Thus, the presence of both direct and indirect bandgaps can contribute to the overall absorption properties of the semiconductor across a broader range of the solar spectrum.

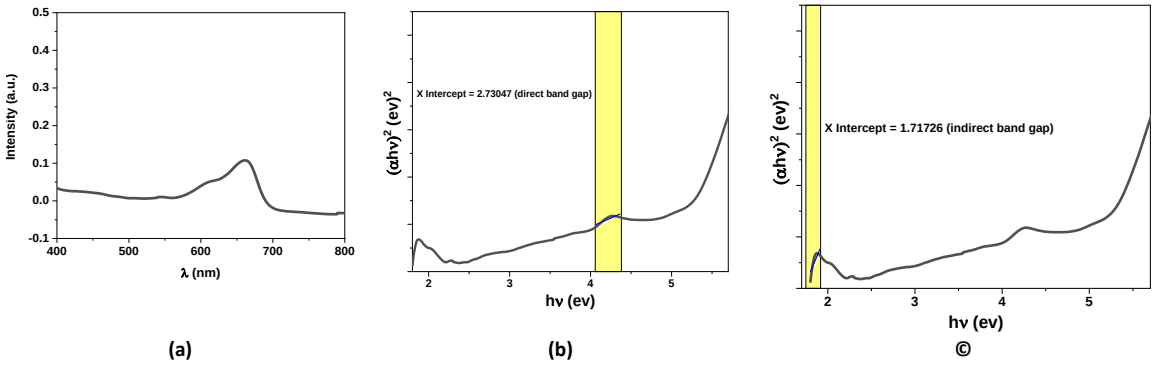

Fig. (6): CTAB@$CoFe_2O_4$ NC UV-Vis absorption spectrum (a), Tauc plot of direct band gap (b) Tauc plot of indirect band gap (c).

3.2. Photocatalytic Reduction of Cr(VI)

Various conditions control the photoreduction of Cr (VI), especially the amount of catalyst, the pH of the solution, and the contact time. Furthermore, CTAB modification changes the surface charge of $CoFe_2O_4$ NPs to positive, enabling efficient Cr(VI) reduction through electrostatic interactions.

In all experiments, there was always a dark control (DC) experiment using the catalyst and a light control (LC) in which light applied without any catalyst.

3.2.1. Effect of Catalyst Concentration

The influence of the catalyst amount is a very essential parameter. Results in **Fig. (7)** indicated that as the catalyst concentration increases, the reduction efficiency also increases. This is because a higher concentration of catalyst provides more active binding sites for the reactants, leading to faster and more efficient reactions. The reduction efficiency as a function of catalyst concentration was carried out applying 3 different catalyst amounts (1, 3, and 5mg/mL) as a function of time (0-150 min). The photoreduction efficiency is calculated according to Eq (1) [2].

$$Photoreduction\,\% = \frac{C_0 - C_t}{C_0}\,X\,100 \qquad (1)$$

where C_0 and C_t are the initial and final concentration (after time t) of Cr (VI) in the solution. The effect of CTAB@$CoFe_2O_4$ NC dose on the photoreduction of Cr(VI) is shown in **Fig.(7)**.

It was noticed that the photoreduction rate increases with increasing the catalyst concentration and the contact time. The Cr(VI) reductionincreased from 45% to 78 % when increasing the CTAB@$CoFe_2O_4$ NC from 1 to 3 mg/mL. Similar effect was reported in [25] when they found that the photodegradation rate of Cr(VI) enhanced with the increase in $CoFe_2O_4$ catalyst amount due to more surface and photocatalytic active sites. However, 3mg/mL catalyst dose can be considered as an optimal concentration beyond which further increases to 5 mg/mL may not provide significant improvements (85%). The photocatalysis operational cost is also directly affected by the catalyst concentration, making it important to strike a balance between efficiency and cost.

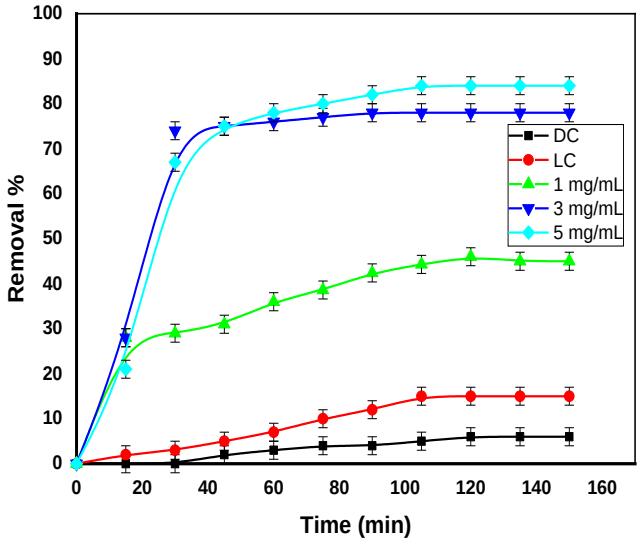

Fig. (7): The photoreduction of Cr(VI) at different catalyst concentrations (1, 2, and 3 mg/mL) and pH 5.

3.2.2. Effect of pH

Solution pH plays a crucial role in the photoreduction of metal ions, such as Cr(VI). It affects the surface charge of the adsorbent and the presence of functional groups, which in turn influence the adsorption and reduction processes. The results in **Fig. (8)** indicate that decreasing the pH significantly increases the photoreduction rate. This could be attributed to the interaction between the negatively charged Cr(VI) ions and the protonated (highly positive) surface of the catalyst at lower pH levels. The stronger attraction between the Cr(VI) ions and the catalyst surface leads to enhanced adsorption, promoting photocatalytic reduction efficiency. At pH 3 with 3 and 5 mg/mL catalyst amount, the photoreduction efficiency reaches 99% after 90 minutes approaching the complete reduction of Cr(VI). This result was confirmed by ionic chromatography analysis of the Cr(VI) concentrations before and after photocatalytic degradation by CTAB/$CoFe_2O_4$ NC photocatalyst (Fig. S1 (a) and (b) respectively, supplementary file). The figure illustrates the detection of the Cr(VI) in water samples after 5.03 minutes, which is consistent with the literature [32]. It also confirms that the remaining concentration Cr(VI) after photocatalytic degradation applying CTAB/$CoFe_2O_4$ NC and DPC for 150 minutes was found to be 1%.

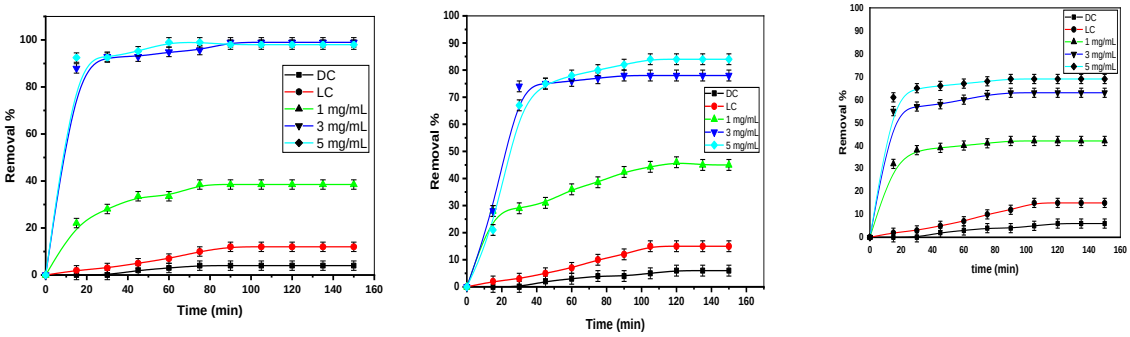

(a) (b) ©

Fig. (8): The photoreduction of Cr(VI) (10^{-3} M/L) applying CTAB@$CoFe_2O_4$ NC at different pH (a) pH3, (b) pH5, and (c) pH7, and different catalyst concentration 1, 3 and 5 mg/mL and

Indeed, increasing the pH of the solution can lead to a reduction in the fprotonation of the catalyst surface and subsequently decrease the electrostatic attraction between Cr(VI) ions and the CTAB@$CoFe_2O_4$ NC catalyst. This in turn can result in a decrease in the photocatalytic reduction efficiency of Cr(VI). Thus the photocatalytic reduction of Cr(VI) decreased from 99% at pH 3 to 85% at pH 5 and 70% at pH 7. These results agree with the findings of [33] for the photocatalytic reduction of Cr(VI) using Ce-ZrO2 under visible light. These findings highlight the importance of pH control in optimizing the photocatalytic reduction process of Cr(VI).

3.2.3. Catalyst Recycling

The reuse of CTAB@$CoFe_2O_4$ NC was investigated in this study for photocatalytic reduction of Cr(VI) for four successive cycles. The photoreduction rate percentage was calculated according to Eq (2)[34].

$$R_r = \frac{C_r}{C_0} x100 \quad (2)$$

Where R represents the photoreduction ratio %, r is the cycle number, C0 is the photoreduction efficiency in the first cycle, and Cr is the photoreduction efficiency at the second, third or fourth cycle. **Fig. (9)** displays the photoreduction ratio percentage of Cr(VI) using CTAB/$CoFe_2O_4$ NC at pH3 for four successive cycles. The figure illustrates that the photoreduction ratio percentage of CTAB/$CoFe_2O_4$ NC does not change in the four cycles. This could be due to maintaining the reactivity of $CoFe_2O_4$ NPs by protection capping with CTAB. Another study also noticed that there is no change in the photocatalytic activity of the $CoFe_2O_4$ NPs when combined with polyaniline for the removal of anionic dyes over 3 successive cycles[35].

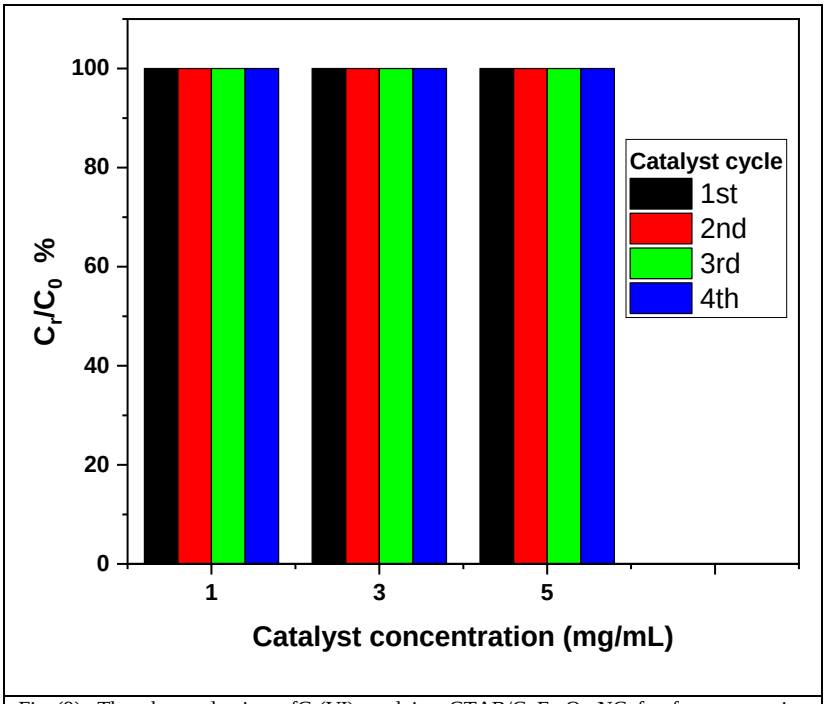

Fig (9): The photoreduction ofCr(VI) applying CTAB/$CoFe_2O_4$ NC for four successive cycles at 3 different catalyst doses (1, 3, and 5 mg/mL) and pH3.

Table (1) shows a collective summary of all results at different pH levels and different CTAB/$CoFe_2O_4$ NC photocatalyst dose after 150 minutes.

Factor / Concentration	1 mg/ml Removal %	3 mg/ml Removal %	5 mg/ml Removal %
Dark control	5	5	5
Light control	10	10	10
pH 7	42	63	69
pH 5	45	78	84
pH 3	38	99	99

4. Conclusion:

The CTAB/$CoFe_2O_4$ NC photocatalyst presents a promising solution for addressing the challenge of Cr(VI) contamination in water. It was synthesized by coprecipitation in an alkaline medium. The FTIR analysis revealed that there is an electrostatic attraction as well as hydrogen bonding between the $CoFe_2O_4$ surface hydroxyl groups and the ammonium moiety in CTAB. XRD and TEM analyses confirmed the cubic crystallite shape and average size (20 nm) of the CTAB/$CoFe_2O_4$ NC. The photocatalytic reduction experiment showed that 3 mg/mL of CTAB/$CoFe_2O_4$ NC can completely reduce Cr(VI) from the sample under acidic pH3 conditions after 150 minutes reduction time. Additionally, CTAB/$CoFe_2O_4$ NC was successfully recycled without affecting the effectiveness of Cr(VI) reduction throughout the tested cycles. This method differs from others as it not only removes Cr(VI), but also changes its chemical composition. The significance of this method lies in the transformation of Cr(VI) into a non-toxic form, avoiding the health risks associated with Cr(VI) water contamination, making it highly beneficial.

Conflict of interest

The authors have no conflict of interest to declare.

Formatting of funding sources

This research did not receive any specific grant from funding agencies in the public, commercial, or not-for-profit sectors.

Acknowledgment

This work was supported by the National Institute of Laser Enhanced Sciences (NILES), Cairo University.

References

[1] M. Zedan, X. Li, R. M. Amin, S. A. ElFeky, and A. F. Zedan, 'Photodeposited Silver versus Gold over g-C3N4 toward Photocatalytic Oxidation of Organic Water Pollutants', *Egypt J Chem*, vol. 65, no. 13, pp. 119–136, 2022, doi: 10.21608/EJCHEM.2022.117227.5293.

[2] H. A. Elbadawy, A. El-Dissouky, S. M. Hussein, S. R. El-Kewaey, S. A. Elfeky, and G. El-Ghannam, 'A novel terpolymer nanocomposite (carboxymethyl β-cyclodextrin–nano chitosan–glutaraldehyde) for the potential removal of a textile dye acid red 37 from water', *Front Chem*, vol. 11, 2023, doi: 10.3389/fchem.2023.1115377.

[3] A. Ngo, H. Nguyen, and D. Hollmann, 'Criticial Assessment of the Photocatalytic Reduction of Cr(VI) over Au/TiO2', *Catalysts*, vol. 8, no. 12, p. 606, Dec. 2018, doi: 10.3390/catal8120606.

[4] M. Costa, 'Toxicity and carcinogenicity of Cr(VI) in animal models and humans.', *Crit Rev Toxicol*, vol. 27, no. 5, pp. 431–42, Sep. 1997, doi: 10.3109/10408449709078442.

[5] F. Mushtaq, X. Chen, A. Veciana, M. Hoop, B. J. Nelson, and S. Pané, 'Magnetoelectric reduction of chromium(VI) to chromium(III)', *Appl Mater Today*, vol. 26, p. 101339, Mar. 2022, doi: 10.1016/j.apmt.2021.101339.

[6] M. Ahmed *et al.*, 'Recent developments in hazardous pollutants removal from wastewater and water reuse within a circular economy', *NPJ Clean Water*, vol. 5, no. 1, p. 12, Apr. 2022, doi: 10.1038/s41545-022-00154-5.

[7] E. N. Zare *et al.*, 'An overview on non-spherical semiconductors for heterogeneous photocatalytic degradation of organic water contaminants', *Chemosphere*, vol. 280, p. 130907, Oct. 2021, doi: 10.1016/j.chemosphere.2021.130907.

[8] A.-S. A. , Al-Sherbini, G. El-Ghannam, H. Yehya and, and O. A. Nassef, 'Optical and magnetic studies of Fe3O4/Au Core/Shell nanocomposites', *Int J Nanosci*, 2019.

[9] D. Uzunoğlu, M. Ergüt, P. Karacabey, and A. Özer, 'Synthesis of cobalt ferrite nanoparticles via chemical precipitation as an effective photocatalyst for photo Fenton-like degradation of methylene blue', *Desalination Water Treat*, vol. 172, pp. 96–105, 2019, doi: 10.5004/dwt.2019.24942.

[10] Sonu *et al.*, 'Review on augmentation in photocatalytic activity of CoFe2O4 via heterojunction formation for photocatalysis of organic pollutants in water', *Journal of Saudi Chemical Society*, vol. 23, no. 8, pp. 1119–1136, Dec. 2019, doi: 10.1016/j.jscs.2019.07.003.

[11] S. A. Elfeky, S. E. Mahmoud, and A. F. Youssef, 'Applications of CTAB modified magnetic nanoparticles for removal of chromium (VI) from contaminated water', *J Adv Res*, vol. 8, no. 4, pp. 435–443, 2017, doi: 10.1016/j.jare.2017.06.002.

[12] M. Gardner and S. Comber, 'Determination of trace concentrations of hexavalent chromium', *Analyst*, vol. 127, no. 1, pp. 153–156, Jan. 2002, doi: 10.1039/b109374f.

[13] S. Das, M. Bououdina, and C. Manoharan, 'The influence of cationic surfactant CTAB on optical, dielectric and magnetic properties of cobalt ferrite nanoparticles', *Ceram Int*, vol. 46, no. 8, pp. 11705–11716, Jun. 2020, doi: 10.1016/j.ceramint.2020.01.202.

[14] M. Haneef, I. H. Gul, M. Hussain, and I. Hassan, 'Investigation of Magnetic and Dielectric Properties of Cobalt Cubic Spinel Ferrite Nanoparticles Synthesized by CTAB-Assisted Co-precipitation Method', *J Supercond Nov Magn*, vol. 34, no. 5, pp. 1467–1476, May 2021, doi: 10.1007/s10948-021-05869-z.

[15] N. M. Hosny, A. Hazem, and S. M. N. Moalla, 'Synthesis, characterization and analytical applications of cobalt ferrite nanoparticles', *Chemical Data Collections*, vol. 42, p. 100948, Dec. 2022, doi: 10.1016/j.cdc.2022.100948.

[16] A. L. Lopes-Moriyama, V. Madigou, C. P. de Souza, and C. Leroux, 'Controlled synthesis of CoFe2O4 nano-octahedra', *Powder Technol*, vol. 256, pp. 482–489, Apr. 2014, doi: 10.1016/j.powtec.2014.01.080.

[17] M. Vadivel, R. R. Babu, K. Ramamurthi, and M. Arivanandhan, 'CTAB cationic surfactant assisted synthesis of CoFe2O4 magnetic nanoparticles', *Ceram Int*, vol. 42, no. 16, pp. 19320–19328, Dec. 2016, doi: 10.1016/j.ceramint.2016.09.101.

[18] A. Lace, D. Ryan, M. Bowkett, and J. Cleary, 'Chromium Monitoring in Water by Colorimetry Using Optimised 1,5-Diphenylcarbazide Method', *Int J Environ Res Public Health*, vol. 16, no. 10, p. 1803, May 2019, doi: 10.3390/ijerph16101803.

[19] J. Bayuo, M. A. Abukari, and K. B. Pelig-Ba, 'Desorption of chromium (VI) and lead (II) ions and regeneration of the exhausted adsorbent', *Appl Water Sci*, vol. 10, no. 7, p. 171, Jul. 2020, doi: 10.1007/s13201-020-01250-y.

[20] W. Li, F. Xiao, H. Su, D. Wang, and X. Yang, 'Investigation of adsorption and photocatalytic activities of in situ cetyltrimethylammonium bromide-modified Bi/BiOCl heterojunction photocatalyst for organic contaminants removal', *RSC Adv*, vol. 6, no. 96, pp. 93309–93317, 2016, doi: 10.1039/C6RA19904F.

[21] B. H. Stuart, *Infrared Spectroscopy: Fundamentals and Applications*. Wiley, 2004. doi: 10.1002/0470011149.

[22] S. Bhattacharjee, 'DLS and zeta potential – What they are and what they are not?', *Journal of Controlled Release*, vol. 235, pp. 337–351, Aug. 2016, doi: 10.1016/j.jconrel.2016.06.017.

[23] S. Betal, M. Dutta, L. F. Cotica, A. Bhalla, and R. Guo, '$BaTiO_3$ Coated $CoFe_2$ O $_4$ –Core-Shell Magnetoelectric Nanoparticles (CSMEN) Characterization', *Integrated Ferroelectrics*, vol. 166, no. 1, pp. 225–231, Oct. 2015, doi: 10.1080/10584587.2015.1092653.

[24] N. Wu *et al.*, 'Ultrathin high-performance electromagnetic wave absorbers with facilely fabricated hierarchical porous Co/C crabapples', *J Mater Chem C Mater*, vol. 7, no. 6, pp. 1659–1669, 2019, doi: 10.1039/C8TC04984J.

[25] B. Thomas and L. K. Alexander, 'Enhanced synergetic effect of Cr(VI) ion removal and anionic dye degradation with superparamagnetic cobalt ferrite meso–macroporous nanospheres', *Appl Nanosci*, vol. 8, no. 1–2, pp. 125–135, Feb. 2018, doi: 10.1007/s13204-018-0655-6.

[26] N. Heydari, M. Kheirmand, and H. Heli, 'A nanocomposite of $CoFe_2$ O_4 -carbon microspheres for electrochemical energy storage applications', *Int J Green Energy*, vol. 16, no. 6, pp. 476–482, May 2019, doi: 10.1080/15435075.2019.1580198.

[27] C. Jiang, T. Zhang, S. Li, and Z. Yang, 'A comparative study on Fe(III)-chitosan and Fe(III)-chitosan-CTAB composites for As(V) removal from water: preparation, characterization and reaction mechanism', *Environmental Science and Pollution Research*, vol. 29, no. 51, pp. 77851–77863, Nov. 2022, doi: 10.1007/s11356-022-20701-4.

[28] W. Wang, L. Zhang, Y. Kang, and F. Yu, 'Light-Excited Ag-Doped TiO2−CoFe2O4 Heterojunction Applied to Toluene Gas Detection', *Nanomaterials*, vol. 11, no. 12, p. 3261, Nov. 2021, doi: 10.3390/nano11123261.

[29] S. A. Z. and D. J. D. Steven S. Zumdahl, 'Chemistry ', in *Problems Solution*, 10th ed., S. A. Z. D. J. D. Steven S. Zumdahl, Ed., 2018.

[30] R. Liu *et al.*, 'Recent advancements in g-C_3 N_4 -based photocatalysts for photocatalytic CO_2 reduction: a mini review', *RSC Adv*, vol. 10, no. 49, pp. 29408–29418, 2020, doi: 10.1039/D0RA05779G.

[31] S. Hoang and P. Gao, 'Nanowire Array Structures for Photocatalytic Energy Conversion and Utilization: A Review of Design Concepts, Assembly and Integration, and Function Enabling', *Adv Energy Mater*, vol. 6, no. 23, Dec. 2016, doi: 10.1002/aenm.201600683.

[32] V. Kaur and A. K. Malik, 'Speciation of Chromium Metal Ions by RP-HPLC', *J Chromatogr Sci*, vol. 47, no. 3, pp. 238–242, Mar. 2009, doi: 10.1093/chromsci/47.3.238.

[33] F. E. Bortot Coelho, V. M. Candelario, E. M. R. Araújo, T. L. S. Miranda, and G. Magnacca, 'Photocatalytic Reduction of Cr(VI) in the Presence of Humic Acid Using Immobilized Ce-ZrO_2 under Visible Light.', *Nanomaterials (Basel)*, vol. 10, no. 4, Apr. 2020, doi: 10.3390/nano10040779.

[34] N. A. E. Emara, R. M. Amin, A. F. Youssef, and S. A. Elfeky, 'Recycling of Steel Industry Waste Acid in the Preparation of Fe3O4 Nanocomposite for Heavy Metals Remediation from Wastewater', *Revista de Chimie*, vol. 71, no. 12, pp. 34–46, Jan. 2021, doi: 10.37358/RC.20.12.8384.

[35] P. Xiong, Q. Chen, M. He, X. Sun, and X. Wang, 'Cobalt ferrite–polyaniline heteroarchitecture: a magnetically recyclable photocatalyst with highly enhanced performances', *J Mater Chem*, vol. 22, no. 34, p. 17485, 2012, doi: 10.1039/c2jm31522j.